JOURNAL OF GEOPHYSICAL RESEARCH, VOL. ???, XXXX, DOI:10.1029/,

Radial dependence of CME propagation speed in interplanetary space

M. Yamashita, M. Tokumaru, M. Kojima, and K. Fujiki

Solar-Terrestrial Environment Laboratory, Nagoya University, Japan

---

M. Yamashita, Solar-Terrestrial Environment Laboratory, Nagoya University, 3-13 Honohara, Toyokawa 442-8507, Japan (fujiki@stelab.nagoya-u.ac.jp, kojima@stelab.nagoya-u.ac.jp, tokumaru@stelab.nagoya-u.ac.jp, yamasita@stelab.nagoya-u.ac.jp)

Abstract. We studied radial variation of coronal mass ejection (CME) speeds between the Sun and the Earth orbit using interplanetary scintillation (IPS) measurements at 327 MHz. We analyzed here nine Earth-directed CME events which occurred between 1997 and 2002. Using the enhancement factor of solar wind density fluctuation level (g-value), derived from IPS measurements, we performed a model-fitting analysis of three dimensional CME structure and estimated CME locations in the ambient solar wind. Combining the IPS measurements with coronagraph measurements and near-Earth in situ observations, CME speeds were derived at distances from the Sun to the Earth orbit. The results show that (1) a fast CME is significantly decelerated during the propagation while a slow CME is accelerated, (2) the acceleration and deceleration is mostly was completed by 0.7 AU, and the CME attains nearly the same speed as that of the ambient solar wind. We found that the deceleration rate of the fast CME inversely correlated with the initial speed difference between CMEs and the ambient solar wind. This implies that propagation dynamics of fast CMEs is governed by retardation force caused by interaction with the ambient solar wind, and this supports the aerodynamic drag force model.

1. Introduction

Since coronal mass ejections (CMEs) seriously affect the geospace environment, and a fuller elucidation of their physical processes, including generation, propagation, interaction with solar wind and Earth's magnetosphere, keenly needed from the viewpoint of space weather. In particular, the dynamics of CME propagation between the Sun and the Earth orbit is not well understood, although this understanding is key information for predicting space weather accurately. A main difficulty preventing us from solving this problem is the shortage of CME observational data in the solar wind because most of observations have been performed in the ecliptic plane at near Earth. Although high-cadence image data of CMEs are available from observations by the Large Angle and Spectrometric Coronagraph Experiment (LASCO) [Brueckner et al., 1995] onboard the Solar and Heliospheric Observatory (SOHO) spacecraft since 1996, the field-of-view is limited to within 30 solar radii. To obtain information on CMEs beyond this distance, one must rely on in situ measurements which are distributed sparsely in the heliosphere.

Earlier studies using coronagraph and in situ observations revealed that CMEs undergo significant evolution of propagation speeds between the corona and 1 AU. Lindsay et al. (1999) investigated the relation between the propagation speeds of CME in corona observed by the Solwind and the Solar Maximum Mission (SMM) and those of interplanetary counterpart of CME (ICME) observed by the Helios 1 and the Pioneer Venus Orbiter. As a result, they found that CME speeds near the Sun correlated with ICME speeds observed at 0.7 to 1 AU. An important point to note is that the speed range of ICME is greatly different from that of CME near the Sun. Most of ICME speeds ranged from 300 km/s

to 800 km/s, while CME speeds near the Sun showed a large scatter spanning from less than 50 km/s to greater than 2000 km/s. This means that slow CMEs are accelerated and fast CMEs are decelerated as they propagate in the IP space between the Sun and the Earth. Gopalswamy et al. (2000) determined acceleration and deceleration rates for 28 CME events observed for 1996–1998 under an assumption that the rate was constant during the propagation. As a result, they found a linear correlation between initial speeds and the acceleration/deceleration rate and a critical velocity of 405 km/s which delineates acceleration and deceleration.

This study aims to derive the radial variation of CME speeds between the Sun and the Earth orbit by combining interplanetary scintillation (IPS) observations with coronagraph and in situ observations. IPS observations using many radio sources are useful to study global properties of a transient solar wind stream such as a CME, since they allow us to probe multiple points in the inner heliosphere in a short time. IPS observations used here are sensitive to the solar wind between the corona and the Earth orbit, therefore they bridge the gap in CME observations. The utility of IPS observations was demonstrated by some earlier CME studies. For example, propagation of the 2000 July 14 halo CME between the Sun and the Earth orbit was successfully tracked using IPS observations made with the Ooty radio-telescope (Manoharan et al., 2001). In the present study, we analyzed our IPS observations for nine Earth-diretcted CME events during 1997–2002. In this analysis, line-of-sight (LOS) integration effects inherent in IPS observations were carefully treated to obtain precise estimates of CME speeds between the Sun and the Earth orbit.

The outline of this paper is as follows. In section 2, we introduce the observations used for this study. In section 3, we describe the method to estimate CME speeds between the corona and 1 AU from these observations. In section 4, we describe the radial variation of CME speeds obtained here. In section 5, we the examine the relation among the acceleration/deceleration profile, initial CME speeds, and ambient solar wind speeds. In section 6, we summarize the result.

2. IPS Observations

Regular IPS observations with 327 MHz system have been made at the Solar-Terrestrial Environment Laboratory (STEL) , Nagoya University (Kojima and Kakinuma, 1990). The STEL IPS observations cover the radial distance range between 0.2 and 0.9 AU, and nearly 40 IPS radio sources are observed daily between April and December. Solar wind speeds and density disturbance factors (so called g-values; Gapper et al., 1982) are derived from the IPS observations. The g-value is related to the level of solar wind (electron) density fluctuations ΔN_e through the following integration equation:

$$g^2 = K \int_0^\infty \Delta N_e^2 w(z) dz \tag{1}$$

where $w(z)$ is the IPS weighting function, z is the distance from the earth along a LOS, and K is a factor to normalize with undisturbed solar wind level: the g-value of undisturbed solar wind is ~ 1, and $g > 1$ means the excess of ΔN_e over the average level. The g-values are particularly useful to detect a CME, since they show an abrupt increase, when dense plasmas associated with it pass across the LOS. In this study, we analyzed the g-value data obtained from STEL IPS observations.

We can roughly infer the spatial distribution of CMEs from plane-of-sky distribution of enhanced g-value. However, the estimated distribution is significantly influenced by the LOS integration effect. Since this inferred distribution is plane-of-sky projection of three-dimensional CME structure, we have to deconvolve the LOS integration to retrieve the 3D CME structure. In this study, we performed deconvolution analysis of g-value data by fitting a three-dimensional ΔN_e model to observations. We assumed here a shell-shape distribution of ΔN_e enhancement defined by

$$\Delta N_e = \frac{C}{r^2}(f_{enh} \exp(-(\frac{r - r_0}{dr})^2) \exp(-(\frac{\theta}{d\theta})^2) + 1) \quad (2)$$

where r is the radial distance, θ is the separation angle to the central axis, f_{enh} is a peak value of ΔN_e enhancement, r_0 is the radial distance of the ΔN_e enhancement peak, dr is the e-folding radial thickness, $d\theta$ is the e-folding angular extent, and C is a constant. A schematic illustration of the ΔN_e model is shown in Figure 1. In this model, the ΔN_e enhanced region, which represented a CME, was assumed to expand radially at a constant speed during IPS observations for a given day. Here, a typical value of 500 km/s was used for the expansion speed, since a result was not so sensitive to this parameter. Thus, the ΔN_e model was defined by six free parameters: r_0, f_{enh}, dr, $d\theta$, and the heliographic coordinate of the center axis (λ, ϕ). Among these parameters, r_0 is the most important in this study, since it enables the determination of CME propagation speeds in the solar wind (see the next section).

We calculated a g-value using the ΔN_e model and Eq. (1) for each LOS. The free parameters were adjusted to minimize the rms deviation χ^2 between observed and calculated

g-values, which was given by

$$\chi^2 = \sum_{i=1}^{n} (g_{obs}^2(i) - g_{cal}^2(i))^2 / g_{cal}(i) \quad (3)$$

where n is the number of LOS, and g_{cal}, g_{obs} are calculated and observed g-values. The best-fit model obtained through this process represents the three-dimensional feature of CME.

Figure 2 shows an example of IPS observations for a CME event and the best-fit model obtained from our analysis. The left panel of the figure is a sky projection map of g-values observed for the period between July 11 23-h and July 12 7-h UT, 2000. The center of this map corresponds to the location of the Sun, and the horizontal and vertical axes are parallel to the east-west and north-south direction. Dotted concentric circles indicate radial distances of 0.3, 0.6 and 0.9 AU. Solid circles indicate plane-of-sky locations of the observed g-values, and a radius of each circle represents intensity of the observed g-value. As shown in the map, many g-value enhancements were observed in the northeast quadrant of the sky plane. These enhancements were interplanetary consequences of the partial halo CME event, which was observed on July 10, 2000 21:50 UT by the LASCO C2 coronagraph. The right panel of the figure displays calculations of g-value using the best-fit model for this CME event. It is clearly demonstrated here that the model calculations excellently mimic IPS observations. From this analysis the location of g-value enhancements at 03:00 on July 2000 was determined to be $r_0 = 0.59$ AU for this event. (detailed structure is given by Yamashita et al., (2003))

3. Estimation of CME Speeds between Corona and 1 AU

Once a coronal counterpart of g-value enhancements is determined from coronagraph observations, an average propagation speed of the CME (V_1) for the distance range between the corona and the distance r_0 where the IPS measurements were made derived from the following formula:

$$V_1 = (r_0 - r_{corona})/(T_{IPS} - T_{corona}) \tag{4}$$

where r_{corona} is the radial distance of the CME in the corona, and T_{corona} and T_{IPS} are the reference times of coronagraph and IPS observations, respectively. In the same way, an average propagation speed of CME for the range between r_0 and 1 AU (V_2) can be determined, once a near-Earth counterpart of the CME is identified from in situ measurements:

$$V_2 = (r_{Earth} - r_0)/(T_{Earth} - T_{IPS}) \tag{5}$$

where r_{Earth} and T_{Earth} are the radial distance and reference time of in situ measurements, and $r_{Earth} \simeq 1$ AU. In this study, an arrival time of an IP shock at spacecraft was used as T_{Earth}, since most g-value enhancements represent high density compression regions leading high-speed streams (e.g., Moore and Harrison, 1994).

4. Event Selection

To find the coronal and near-Earth counterparts of g-value enhancements, we basically used the list of IP shocks and associated CMEs compiled by Manoharan et al. (2004). This list includes 91 IP shock events associated with halo CMEs originating within about ± 30 in longitude and latitude from the center of the Sun during 1997–2002. We searched g-value enhancements from our IPS observations, which occurred one or two days before

the IP shock event observed by spacecraft near the earth. For 30 IP shock events out of 91 events, our IPS observations were unavailable owing to either intentional suspension for wintering or accidental interruptions by system failures. For 12 events, no marked g-value enhancements were identified by our IPS observations. The reason for this may be ascribed to insufficient density of LOS or timing of the IPS observations. We performed the model fitting analysis of our g-value data for the remaining 49 events, and successfully obtained the best-fit models for 19 cases of IP shock events. We calculated propagation speeds V_1 and V_2 using Eqs. (4) and (5). Here, we adopted the occurrence times of white-light CME and IP shock in the list as T_{corona} and T_{Earth}, respectively. Since the C2 appearance time was used for T_{corona}, we used the inner boundary of the LASCO C2 field-of-view, $2R_S$, as r_{corona}. We also used the white-light CME speed and the IP shock speed as V_{corona} and V_{Earth}, respectively. Out of the 19 events, 11 cases yielded extraordinary high speeds, which were inconsistent with V_{corona} and V_{Earth}. These could be caused from miss corresponding between the IP shock/white-light CME and g-value enhancement events. Therefore, we discarded these cases, and used the remaining eight cases in this study.

The g-value enhancements were observed between July 11 and 12 in 2000 at the STEL (Figure 2) are not listed in Manoharan et al. (2004), since the source location of CME deviated from the disk-center more then 30 degree. Nevertheless, the IP shock associated with this CME event was evidently observed by in situ measurements at 1 AU. Therefore, we included this event in the present study. We obtained information on the associated white-light CME from the SOHO LASCO CME catalog (http://cdaw.gsfc.nasa.gov/CME_list/index.html). Information on the IP shock associ-

ated with this CME event was adopted from the list of near-Earth interplanetary CMEs produced by Cane and Richardson (2003). The shock passage time at 1 AU of the list was used as T_{Earth}. As the result, we obtained T_{corona} = 21:50 UT on July 10, 2000 and T_{Earth} = 09:42 UT on July 13, 2000, then V_1 = 826 km/s and V_2 = 568 km/s for the g-value enhancement event observed between July 11 and 12.

5. Results

We analyzed our IPS observations for the period between 1997 and 2002, and successfully obtained a set of CME speeds V_{corona}, V_1, V_2 and V_{Earth} for nine events. The results are summarized in Table 1, which includes information on T_{IPS}, r_0, T_{corona}, V_{corona}, T_{Earth}, V_{Earth}, V_{SW}, V_1, r_1, V_2, and r_2. Parameters of r_1 and r_2 are reference distances corresponding to V_1, V_2, and they are given by $r_1 = (r_{corona} + r_0)/2$ and $r_2 = (r_0 + r_{Earth})/2$. V_{SW} is the pre-event level of the solar wind speed (i.e. the speed of the ambient solar wind). We used the solar wind data taken by the Advanced Composition Explorer (ACE) spacecraft (http://www.srl.caltech.edu/ACE/ASC/) to determine V_{SW}.

The CME speeds are plotted as a function of the radial distance in Figure 3. The horizontal bars in the figure indicate the distance ranges for which CME speeds were derived. Since the white-light CME speeds V_{corona} were determined from the linear fit to LASCO observations for 2-30 R_S, its reference distance was considered as $16R_S$ = 0.08 AU. As clearly shown here, CME speeds drastically vary during the propagation between the corona and 1 AU. The CMEs with an initial speed faster than 1000 km/s speed are significantly decelerated with increasing distance, while slow ($<$ 400 km/s) CMEs are accelerated. Such evolution results in decrease of CME speed range. In Figure 3, V_{corona} exhibit a large scatter ranging from 100 km/s to 1500 km/s, while V_{Earth} range from 400

km/s to 900 km/s. This fact is consistent with the earlier work done by Lindsay et al. (1999). An important point to note is that our analysis has revealed that most of deceleration/acceleration take place in the near-Sun region and that the speed changes for > 0.7 AU are fairly small.This fact is consistent with the acceleration-cessation distance model proposed by Gopalswamy et al. (2001), in which the effective acceleration/deceleration was assumed to cease at a given distance from the Sun, and CMEs were assumed to travel with a constant speed beyond the distance. According to their study, an acceleration-cessation distance of 0.76 AU was found to represent observations quite well.

In order to clarify the deceleration/acceleration process of CME in interplanetary space, we investigated radial variation of the difference between CME speeds and the ambient solar wind speed (V_{SW}) for each event. In Figure 4, $V - V_{SW}$ is plotted as a function of radial distance r for CME events whose V_{corona} is larger than V_{SW}. Here, V denotes the CME speed (i.e., V_{corona}, V_1, V_2, and V_{Earth}). As shown here, all events exhibit a radial decrease of CME speeds. The important point to note is that the strength of CME deceleration depends on an initial speed difference. Namely, the events with a large speed difference in the corona undergo a strong deceleration, while those with a small speed difference are mildly decelerated. To explore the relation between the initial speed difference and the deceleration rate, we fitted the following function to the observed radial variation of $V - V_{SW}$:

$$V - V_{SW} = \Delta V_0 r^a \tag{6}$$

where r is the radial distance, and ΔV_0 and a are free parameters. The power-law index a represents the strength of deceleration. The solid line in each panel indicates the best-fit curve. For example, we obtained $a = -0.80$ for the case of the 2000 July 9 CME event.

In Figure 5, the power law indices a of the best-fit curves are plotted as a function of the initial speed difference $V_{corona} - V_{SW}$. As shown evidently, the indices a correlated with the initial speed difference. The correlation coefficient between them is -0.459, and the regression line is indicated in the figure by a solid line ($a = -0.0004(V - V_{SW}) - 0.43$).

We also analyzed slow CME events with $V_{corona} < V_{SW}$, in the same way. However, we could not fit Eq. (6) to the observed radial variation of $V - V_{SW}$, since $V_{earth} > V_{SW}$. We discuss slow CME events in the next section.

6. Discussion

The power-law indices a of the radial decrease of CME speeds ranged from -0.1 to -1.2 and inversely correlate with the speed difference between the CME in the corona and the ambient solar wind. In the case of the blast wave model of IP shock propagation proposed by Dryer (1974), the index should be $a = -0.5$. Therefore, the blast wave model can not explain the results obtained here. Our results suggest that the retardation force acting on fast CMEs depends on the speed difference between the CME and the ambient solar wind. This fact supports the aerodynamic drag model proposed by Vršnak and Gopalswamy (2002).

For the three cases of slow CME events, we could not fit Eq. (6) to the observations since the $V - V_{SW}$ of slow CMEs changed its sign during propagation. Namely, CME speeds in the near-Earth solar wind became higher than the ambient ones ($V - V_{SW} > 0$), while those in the corona were lower than the ambient ones ($V - V_{SW} < 0$). Observed radial profiles of CME speed for the slow events suggest that the propelling force continues accelerating the CME until the speed exceeds the ambient one. This can not be explained only by the propelling force caused by an effect of interaction with the ambient solar wind, and it is

somewhat puzzling. Nevertheless, it was reported from some earlier studies (e.g. Sheeley et al., 1985) that some CME events which had slow initial speeds were associated with IP shock waves at larger radial distances. Therefore, we need to explore the propagation dynamics of slow CME events in more detail.

The number of CME events for which we successfully obtained the best-fit model was rather limited to 19 out of 49 events. The reason for this is because we used the oversimplified model for the analysis. The simplified model can not be used for multiple CME events which occurred consecutively in a few days and also for highly anisotropic CME structures.

It was reported that extraordinary fast full-halo CMEs with initial speed of $> 2,000$ occurred on October 28 and 29 in 2003, and they maintained their speeds during propagation between the Sun and the Earth, and no significant deceleration was observed for these events. This fact is inconsistent with what we found from the present study. We consider that the weak deceleration observed for those very fast events might be due to marked a reduction of the ambient solar wind density (Tokumaru et al., 2005), since rarefaction of the ambient solar wind caused by priory event in multi-CME event greatly moderates the drag force acting on CMEs. To verify this hypothesis, we need to examine the relation between the speed variation and the ambient solar wind density carefully in a future study.

In this study, we used the pre-event levels of the solar wind speed measured by spacecraft as V_{SW}. Here, we should note that in situ measurements may not necessarily represent global properties of the ambient solar wind. Solar wind speeds obtained from our IPS observations are considered as useful data for studying global properties. Therefore, com-

parison between CME speed variation and IPS speed data will be a promising future work.

7. Summary

We investigated the radial variation of CME propagation speed in the IP space for nine events, which occurred between 1997 and 2002, using STEL IPS measurements. In this study, we determined 3-dimensional distribution of CME-driven IP disturbances from the model-fitting analysis of g-value data, and then derived average propagation speeds of CMEs in the radial distance range between the corona and 1 AU by combining the g-value data with coronagraph and near-earth in situ observations. The results clearly demonstrated that fast CMEs were decelerated significantly during the propagation and slow ones were accelerated. This fact confirms earlier studies. The point to emphasize here is that we revealed the process of CME speed evolution at multi-distances between the corona and 1 AU by using IPS observations. Our results suggest that deceleration/acceleration almost completed by 0.7 AU. In addition, we found that the deceleration rate of fast CME events with $V_{corona} > V_{SW}$ inversely correlated with the initial speed difference between CMEs and the ambient solar wind. We fitted the power-law function to the observed radial variation of CME speeds for fast events, and obtained the indices varied from -0.1 to -1.2 with increasing the speed difference. The regression line between $V - V_{SW}$ and a was $a = -0.0004(V - V_{SW}) - 0.43$. This result suggest that propagation dynamics of fast CMEs in the solar wind are dominated by the retardation force exerted by the speed difference to the ambient solar wind, and this finding is basically consistent with the aerodynamic drag force model.

Acknowledgments. The ACE data were downloaded from the website of the Space Radiation Laboratory (http://www.srl.caltech.edu/ACE). The CME catalog is generated and maintained by NASA and The Catholic University of America in cooperation with the Naval Research Laboratory. SOHO is a project of international cooperation between ESA and NASA.

References

Brueckner, G. E., et al. (1995), The large angle spectroscopic coronagraph (LASCO), *Sol. Phys., 162*, 357.

Cane, H. V. and I. G. Richardson (2003), Interplanetary coronal mass ejections in the near-Earth solar wind during 1996-2002, *J. Geophys. Res., 108*(A4), 1156, doi:10.1029/2002JA009817.

Dryer, M. (1974), Interplanetary shock waves generated by solar flares, *Space Sci. Rev., 15*, 403.

Gapper, G. R., A. Hewish, A. Purvis, and P. J. Duffet-Smith (1982), Observing interplanetary disturbances from the ground, *Nature, 296*, 633.

Gopalswamy, N., A. Lara, R. P. Lepping, M. L. Kaiser, D. Berdichevsky, and O. C. St Cyr (2000), Interplanetary acceleration of coronal mass ejections, *Geophys. Res. Lett., 27*, 145.

Gopalswamy, N., A. Lara, S. Yashiro, M. L. Kaiser, and R. A. Howard (2001), Predicting the 1-AU arrival times of coronal mass ejections, *J. Geophys. Res., 106*, 29,207.

Kojima M. and T. Kakinuma (1990), Solar cycle dependence of global distribution of solar wind speed, *Space Sci. Rev., 53*, 173

Moore, V. and R.A. Harrison (1994), A characterization of discrete solar wind events detected by interplanetary scintillation mapping, *J. Geophys. Res., 99*, 27.

Lindsay, G. M., J. G. Luhmann, G. T. Russell, and J. T. Gosling (1999), Relationships between coronal mass ejection speeds from coronagraph images and interplanetary characteristics of associated interplanetary coronal mass ejections, *J. Geophys. Res., 104*, 12,515.

Manoharan, P.K. M. Tokumaru, M. Pick, P. Subramanian, F.M. Ipavich, K. Schenk, M.L. Kaiser, R.P. Lepping, and A. Vourlidas (2001), Coronal mass ejection of 2000 July 14 flare event: imaging from near-Sun to Earth environment, *Astrophys. J.,* , 559, 1,180.

Manoharan, P. K., N. Gopalswamy, S. Yashiro, A. Lara, G. Michales, and R. A. Howard (2004), Influence of coronal mass ejection interaction on propagation of interplanetary shocks, *J. Geophys. Res., 109*, A06109, doi:10.1029/2003JA010300.

Sheeley, N. R., Jr., R. A. Howard, M. J. Koomen, D. J. Michels, R. Schwenn, K. H. Muhlhauser, and H. Rosenbauer (1985), Coronal mass ejections and interplanetary shocks, *J. Geophys. Res., 90*, 163.

Tokumaru, M., M. Kojima, K. Fujiki, M. Yamashita, and A. Yokobe (2003), Toroidal-shaped interplanetary disturbance associated with the halo coronal mass ejection event on 14 July 2000, *J. Geophys. Res., 108*(A5), 1220, doi:10.1029/2002JA009574.

Tokumaru, M., M. Kojima, K. Fujiki, M. Yamashita, and D. Baba (2005), Interplanetary consequences caused by the extremely intense solar activity during October-November 2003, *J. Geophys. Res., 110*, A01109, doi:10.1029/2004JA010656.

Vršnak, B., and N. Gopalswamy (2002), Influence of the aerodynamic drag on the motion of interplanetary ejecta, *J. Geophys. Res., 107*(A2), doi:10.1029/2001JA000120.

Figure 1. Schematic illustration of the shell-shape CME model used in this study. The model was defined by six parameters: radial distance r_0, radial thickness dr, angular width $d\theta$, enhancement factor f_{enh}, and coordinates of the center axis (λ, ϕ).

Figure 2. (left) Observed sky projection map of g-value on July 12, 2000 and (right) calculated map using the best-fit models. The dotted circles are constant plane-of-sky distance contours drawn every 0.3 AU. The center of open circles corresponds to the location of LOS. Color and diameter represent a g-value level.

Figure 3. Radial variation of the propagation speed for nine CME events. Symbols connected by dashed lines represent data of a given CME event. Horizontal bars denote the radial distance ranges over which the average speeds were derived.

Figure 4. Distance-speed profiles for fast CME events on (a) 1998/11/07, (b) 1999/08/03, (c) 2000/07/12, (d) 2000/08/09, (e) 2000/09/13, and (f) 2001/04/27. A solid line in each panel shows the power-law function (Eq. (6)) fit to observed data.

Figure 5. Correlation between initial CME speeds in the solar wind frame $\Delta V = V - V_{SW}$ and power-law indices a for six fast CME events. The correlation coefficient between them is -0.459, and a regression line ($a = -0.0004(V - V_{SW}) - 0.43$) is indicated in the figure.

Table 1. Summary of IPS, LASCO and in situ observations for CME events.

IPS			LASCO			in-situ							
T_{IPS}		r_0	T_{corona}		V_{corona}	T_{Earth}		V_{Earth}	V_{sw}	V_1	V_2	r_1	r_2
day	UT	AU	day	UT	km/s	day	UT	km/s	km/s	km/s	km/s	AU	AU
1998/06/12	03h	0.68	06/09	09:27	124	06/13	19:20	409	400	425	330	0.345	0.840
1998/06/24	03h	0.57	06/21	05:35	192	06/25	16:10	471	300	335	481	0.290	0.785
1998/11/07	03h	0.68	11/05	20:44	1118	11/08	04:42	721	500	920	517	0.345	0.840
1999/08/03	03h	0.66	08/01	19:27	1133	08/04	01:46	415	300	856	621	0.335	0.830
1999/09/13	03h	0.46	09/11	01:54	266	09/15	07:43	700	550	381	426	0.235	0.730
2000/07/12	03h	0.59	07/10	21:56	1352	07/13	09:42	700	500	826	567	0.300	0.795
2000/08/09	03h	0.77	08/06	23:06	597	08/10	05:10	428	350	609	365	0.340	0.885
2000/09/13	03h	0.48	09/12	11:54	1550	09/15	04:28	397	550	1293	437	0.245	0.740
2001/04/27	03h	0.41	04/26	12:30	1006	04/28	05:02	820	500	1146	942	0.210	0.705

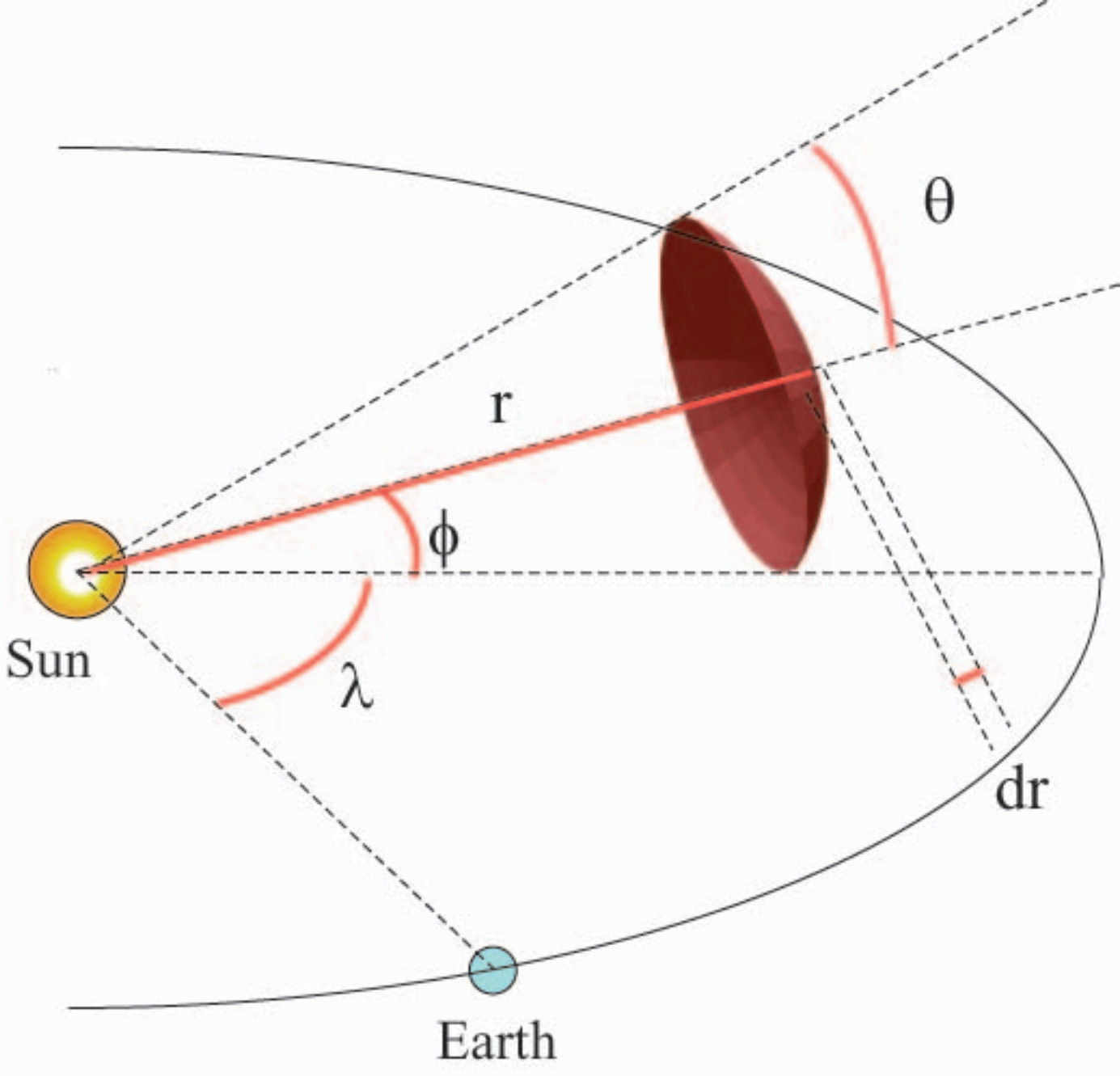
θ
r
ϕ
Sun
λ
dr
Earth

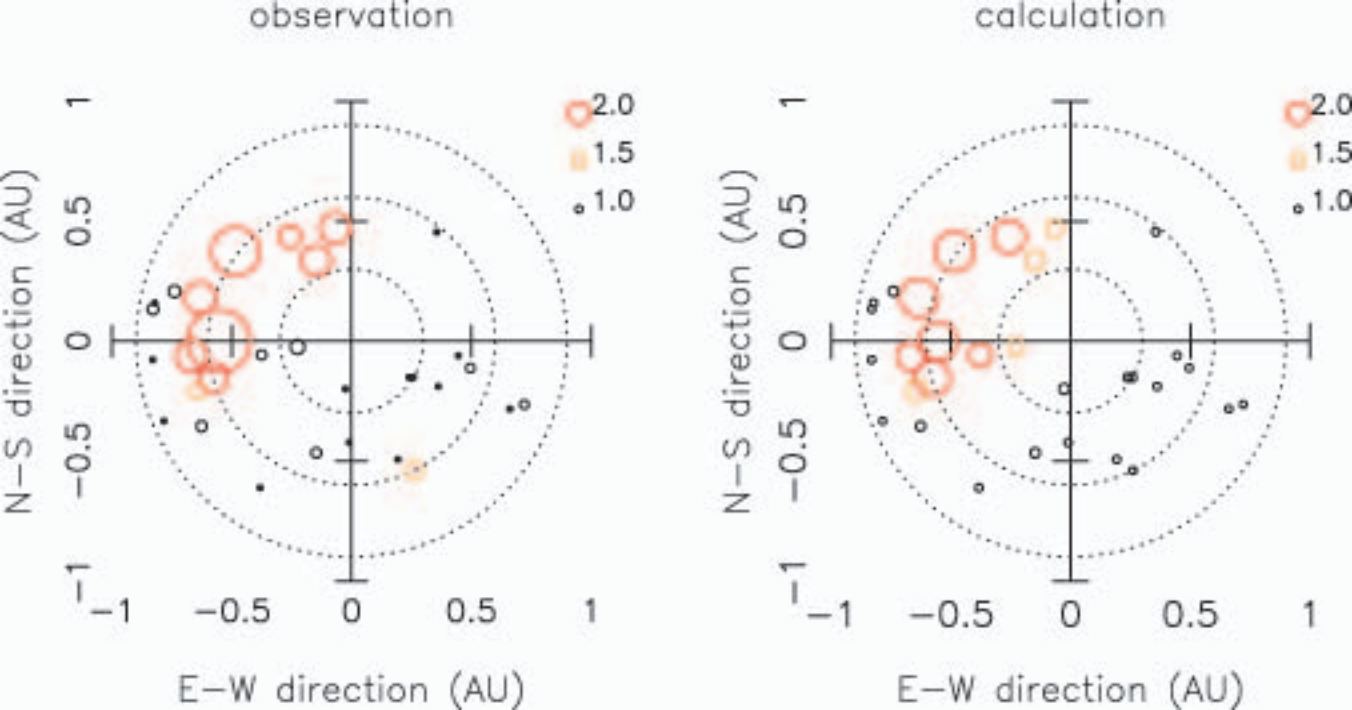
observation
calculation
2.0
1.5
1.0
N−S direction (AU)
E−W direction (AU)
−1
−0.5
0
0.5
1

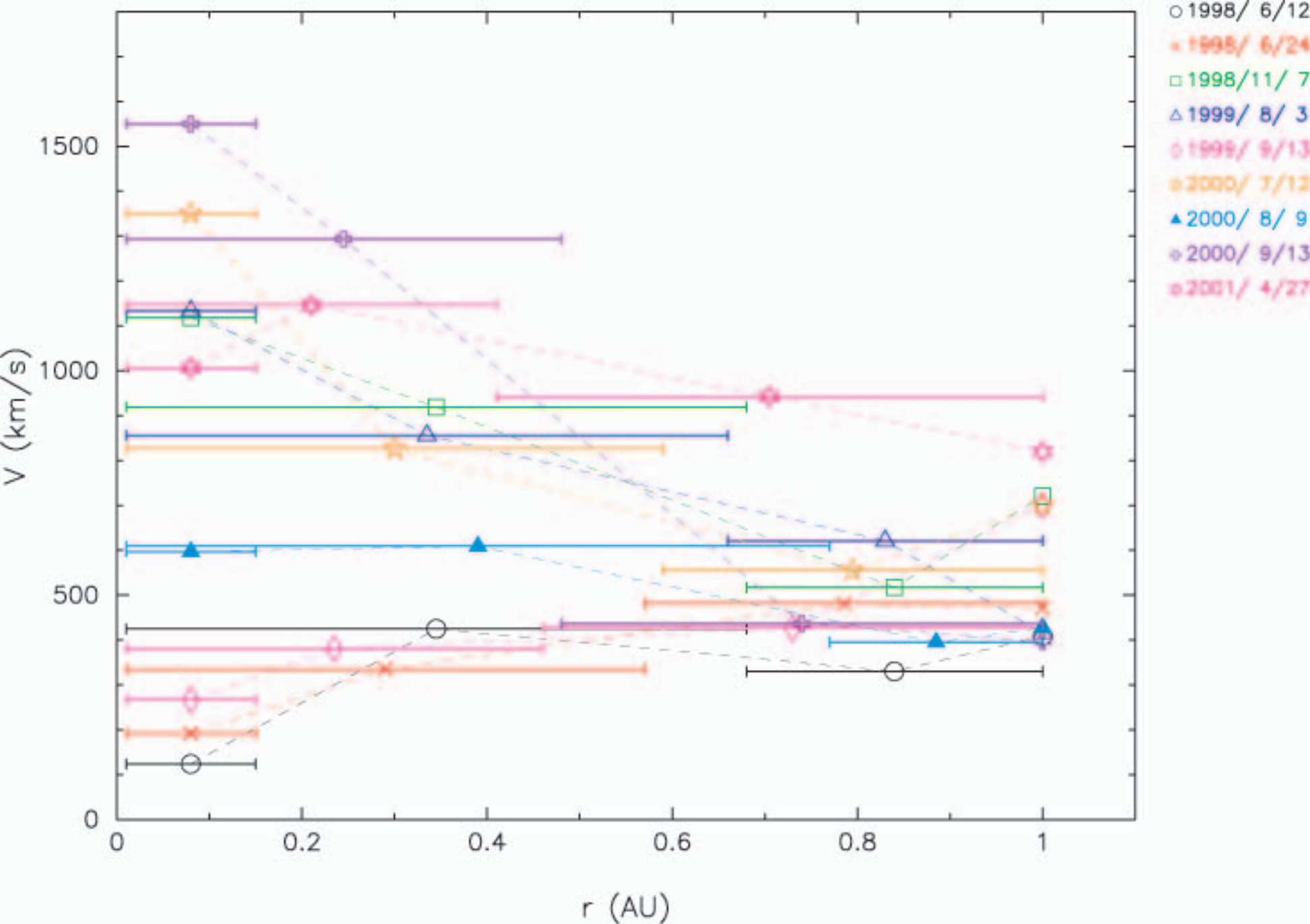
1998/ 6/12
1998/11/ 7
1999/ 8/ 3
2000/ 8/ 9
2000/ 9/13
0
500
1000
1500
V (km/s)
0
0.2
0.4
0.6
0.8
1
r (AU)

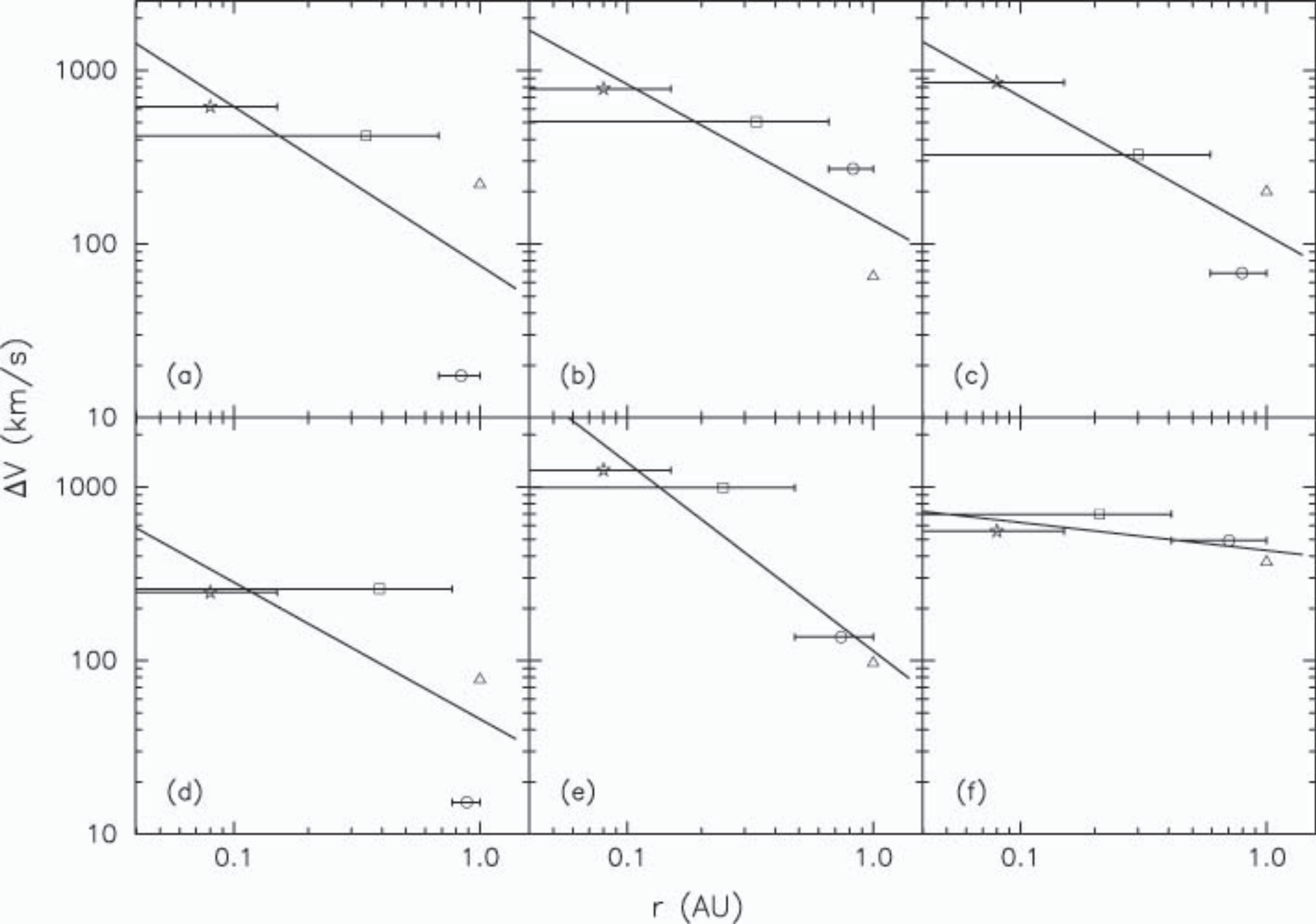
1000
100
10
ΔV (km/s)
(a)
(b)
(c)
(d)
(e)
(f)
0.1
1.0
r (AU)

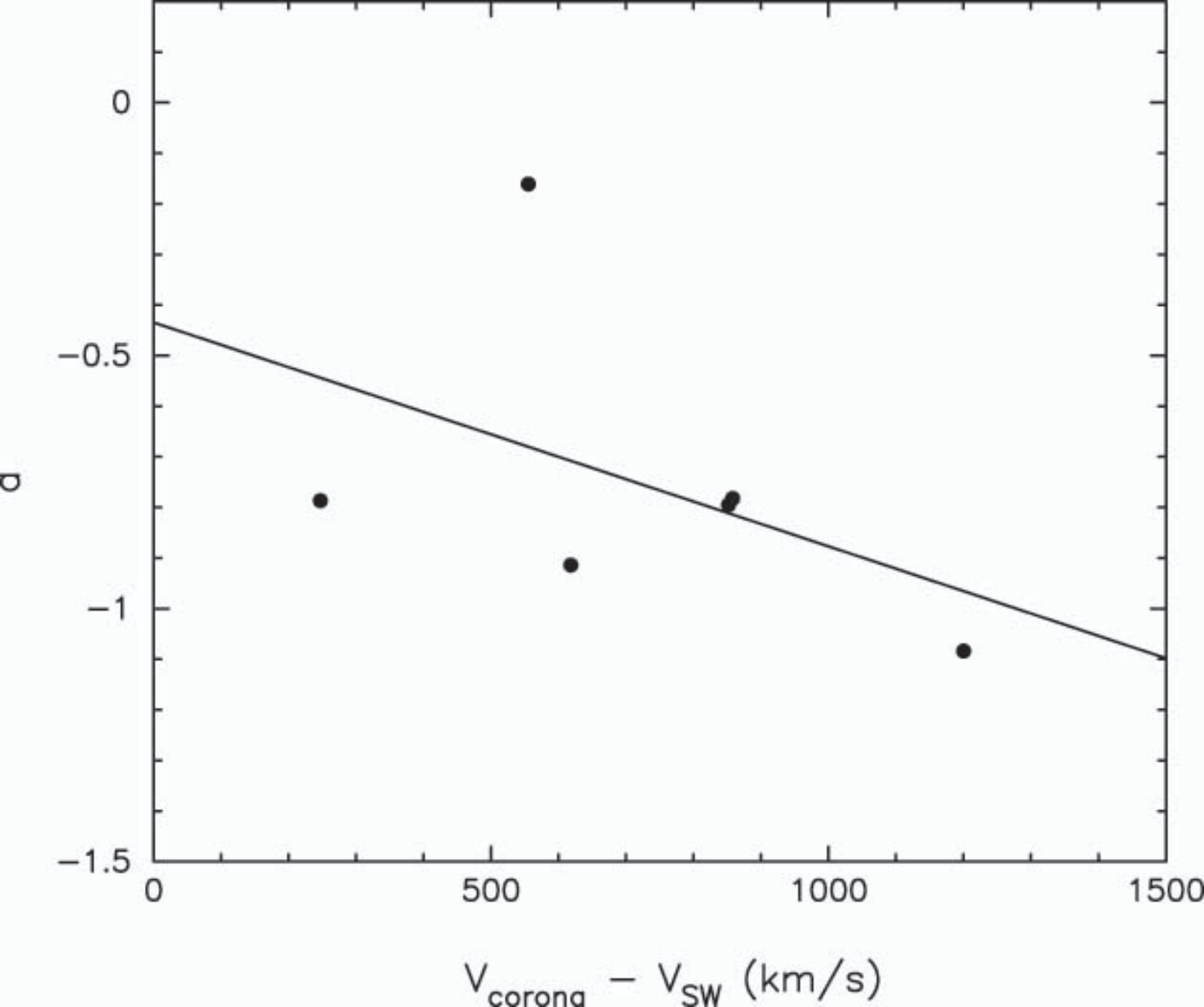
0
−0.5
−1
−1.5
0
500
1000
1500
$V_{corong} - V_{SW}$ (km/s)